JACS
JOURNAL OF THE AMERICAN CHEMICAL SOCIETY
Article
pubs.acs.org/JACS

Three-Coordinate Iron(IV) Bisimido Complexes with Aminocarbene Ligation: Synthesis, Structure, and Reactivity

Lei Wang,[†,§] Lianrui Hu,[‡,§] Hezhong Zhang,[†] Hui Chen,*[,‡] and Liang Deng*[,†]

[†]State Key Laboratory of Organometallic Chemistry, Shanghai Institute of Organic Chemistry, Chinese Academy of Sciences, 345 Lingling Road, Shanghai 200032, P. R. China

[‡]Beijing National Laboratory for Molecular Sciences, CAS Key Laboratory of Photochemistry, Institute of Chemistry, Chinese Academy of Sciences, Beijing 100190, P. R. China

Supporting Information

ABSTRACT: High-valent iron imido species are implicated as reactive intermediates in many iron-catalyzed transformations. However, isolable complexes of this type are rare, and their reactivity is poorly understood. Herein, we report the synthesis, characterization, and reactivity studies on novel three-coordinate iron(IV) bisimido complexes with aminocarbene ligation. Using our recently reported synthetic method for [LFe(NDipp)$_2$] (L = IMes, **1**; Me$_2$-cAAC, **2**), four new iron(IV) imido complexes, [(IPr)Fe(NDipp)$_2$] (**3**) and [(Me$_2$-cAAC)Fe(NR)$_2$] (R = Mes, **4**; Ad, **5**; CMe$_2$CH$_2$Ph, **6**), were prepared from the reactions of three-coordinate iron(0) compounds with organic azides. Characterization data acquired from ^{1}H and ^{13}C NMR spectroscopy, ^{57}Fe Mössbauer spectroscopy, and X-ray diffraction studies suggest a low-spin singlet ground state for these iron(IV) complexes and the multiple-bond character of their Fe−N bonds. A reactivity study taking the reactions of **1** as representative revealed an intramolecular alkane dehydrogenation of **1** to produce the iron(II) complex [(IMes)Fe(NHDipp)(NHC$_6$H$_3$-2-Pr^i-6-CMe=CH$_2$)] (**7**), a Si−H bond activation reaction of **1** with PhSiH$_3$ to produce the iron(II) complex [(IMes)Fe(NHDipp)(NDippSiPhH$_2$)] (**8**), and a [2+2]-addition reaction of **1** with PhNCNPh and *p*-Pr^{i}C$_6$H$_4$NCO to form the corresponding open-shell formal iron(IV) monoimido complexes [(IMes)Fe(NDipp)(N(Dipp)C(NPh)(=NPh))] (**9**) and [(IMes)Fe(NDipp)(N(Dipp)C(O)N(*p*-Pr^{i}C$_6$H$_4$))] (**10**), as well as [NDipp]-group-transfer reactions with CO and Bu^{t}NC. Density functional theory calculations suggested that the alkane chain dehydrogenation reaction starts with a hydrogen atom abstraction mechanism, whereas the Si−H activation reaction proceeds in a [2π+2σ]-addition manner. Both reactions have the pathways at the triplet potential energy surfaces being energetically preferred, and have formal iron(IV) hydride and iron(IV) silyl species as intermediates, respectively. The low-coordinate nature and low d-electron count (d^4) of iron(IV) imido complexes are thought to be the key features endowing their unique reactivity.

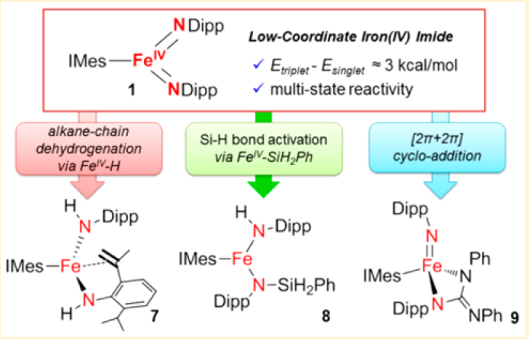

INTRODUCTION

Iron imido species are common intermediates proposed in iron-catalyzed transformations, such as N_2 reduction,[1] C−H bond amination,[2] olefin aziridation,[2a] and aminohydroxylation.[3] Thus, there has been great research interest in their electronic structure and reactivity. In the past century, the chemistry of iron-terminal imido species had remained poorly understood due to the difficulty in accessing them.[4] The field, however, witnessed a surging growth in the recent decade, ever since the report of the first iron-terminal imido complex, [Cl$_3$Fe$_3$(μ_3-NBu^t)$_4$Fe^{IV}(NBu^t)], in 2000.[5] From then until now, more than 40 structurally well-characterized iron-terminal imido compounds have been reported.[6]

High-valent iron imido species are implicated as important intermediates in enzymatic and synthetic nitrene-transfer reactions.[2,7] However, among the reported iron-terminal imido complexes,[5,8−18] structurally well-characterized high-valent iron imido complexes are rare. The first iron(IV)-terminal imido complex, [Cl$_3$Fe$_3$(μ_3-NBu^t)$_4$Fe^{IV}(NBu^t)], reported by Lee, was isolated from the reaction of FeCl$_3$ with LiNHBu^t.[5] Peters and Smith's tetrahedral iron(IV) imido compounds, [{PhBP$^{tBu}_2$(pz^{Me2})}Fe^{IV}(NAd)][BAr$^F_4$][13] and [(triscarbeneborate)Fe^{IV}(NAd)][OTf],[14] respectively, were prepared via the redox reaction of iron(III) imido complexes with ferrocenium cation. Both complexes have an S = 1 ground spin state. Que's six-coordinate species, [(N4Py)Fe(NTs)][OTf]$_2$, was generated by treating [(N4Py)Fe^{II}(NCMe)][OTf]$_2$ with mesityl-*N*-tosylimidoiodinane (MesINTs).[15] The structure of this species is not established by X-ray diffraction, but extensive spectroscopic data support its identity as an iron(IV) imido species with a ground spin state of S = 1. Betley reported a series of four-coordinate high-spin formal iron(IV) imido complexes in the form of [(pyrrol$_2$)Fe(NR)Cl].[16] Characterization data and calculation studies suggest that they are high-spin iron(III) complexes bearing antiferromagnetically

Received: September 11, 2015
Published: October 27, 2015

DOI: 10.1021/jacs.5b09579
J. Am. Chem. Soc. 2015, 137, 14196−14207

coupled imido radicals.[16] Fortier's low-spin (S = 0) iron(IV) imido complex, [(pyrrol$_2$py)Fe^{IV}(NAd)], which has a unique *cis*-divacant octahedral geometry, was prepared from the reaction of an iron(II) precursor with AdN_3.[17] As for isolable iron(V) imido complexes, Power's low-spin (S = 1/2) complex, [(Ar*)Fe^{V}(NAd)$_2$] (Ar* = 3,5-diisopropyl-2,6-di(2′,4′,6′-triisopropylphenyl)phenyl), obtained from the reaction of [(Ar*)Fe^{I}(η^6-C$_6$H$_6$)] with AdN_3, is the solely known example.[18] Despite these elegant synthesis and characterization studies, the reactivity of these high-valent iron imido complexes remains largely unexplored. To our knowledge, the C−H bond amination and olefin aziridation reactions of Betley's imido radical complexes are the only successful explorations into the reactivity of structurally well-defined high-valent iron imido complexes.[16]

The status quo intrigued us and led to our exploration into high-valent iron-terminal imido complexes. Recently, we found that the three-coordinate iron(0) compounds [LFe(η^2:η^2-dvtms)] (L = 1,3-dimesitylimidazol-2-ylidene (IMes) or 3,3,5,5-tetramethyl-1-(2′,6′-diisopropylphenyl)pyrrolidin-2-ylidene (Me$_2$-cAAC); dvtms = divinyltetramethyldisiloxane) can react with 2 equiv of $DippN_3$ (Dipp = 2,6-diisopropylphenyl) to furnish the three-coordinate iron(IV) bisimido complexes [(L)Fe^{IV}(NDipp)$_2$] (L = IMes, **1**; Me$_2$-cAAC, **2**; see Scheme 1)

Scheme 1. Iron(IV) Bisimido Complexes and Their Synthetic Route

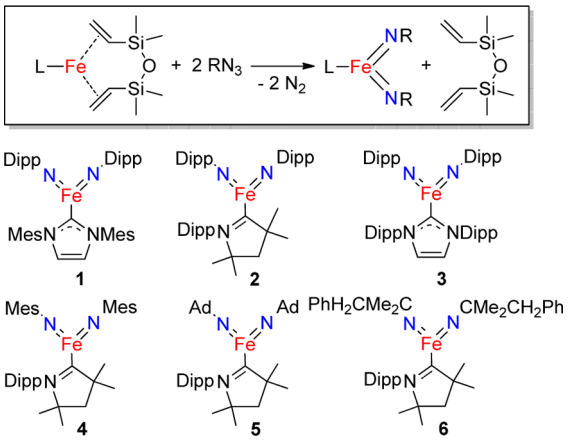

in high yields.[19] The aminocarbene-supported iron imido complexes are unique for their low-coordinate nature and the high valence of the metal center, which might endow these complexes with rich reaction chemistry. In this context, we describe herein (i) a further synthetic study that expands the diversity of three-coordinate iron(IV) bisimides to alkylimido complexes; (ii) a systematic reactivity study on the iron(IV) bisimido complex [(IMes)Fe^{IV}(NDipp)$_2$], which led to the discovery of the novel transformations of iron(IV) imide-facilitated alkane chain dehydrogenation and Si−H bond activation, as well as the [2+2]-cycloaddition with hetero-cumulenes to form iron(IV) monoimido species; and (iii) theoretical studies on the mechanisms of the alkane chain dehydrogenation and Si−H bond activation reactions, which suggest different activation modes (hydrogen atom abstraction versus [2π+2σ]-addition) of the E−H (E = C, Si) bond activation reactions and involvement of iron(IV) hydride and silyl intermediates in the reactions.

RESULTS AND DISCUSSION

Preparation and Characterization of Iron(IV) Bisimido Complexes. The reported synthetic protocol for [(IMes)Fe(NDipp)$_2$] (**1**) and [(Me$_2$-cAAC)Fe(NDipp)$_2$] (**2**)[19] proved applicable for the new three-coordinate iron(IV) bisimido complexes [(IPr)Fe(NDipp)$_2$] (IPr = 1,3-di(2′,6′-diisopropylphenyl)imidazol-2-ylidene, **3**), [(Me$_2$-cAAC)Fe(NMes)$_2$] (Mes = 2,4,6-trimethylphenyl, **4**), [(Me$_2$-cAAC)Fe(NAd)$_2$] (Ad = 1-adamantyl, **5**), and [(Me$_2$-cAAC)Fe(NCMe$_2$CH$_2$Ph)$_2$] (**6**) (Scheme 1). The reactions of [LFe(η^2:η^2-dvtms)] (L = Me$_2$-cAAC or IPr) with the aryl azides, $DippN_3$ and $MesN_3$, proceeded quickly at room temperature, with fast effervescence of N_2 gas, whereas the reactions with the alkyl azides, AdN_3 and $PhCH_2Me_2CN_3$, were slow, and no instant gas evolution was noticed. All the reactions eventually afforded reddish-brown mixtures, from which red or brown crystals of **3**−**6** were isolated in 40−69% yields. Attempts to prepare iron(II) imido intermediates from reactions of the iron(0) complexes with 1 equiv of organic azides generally afforded mixtures of the iron(IV) bisimido complexes with the iron(0) precursors.

Complexes **1**−**6** are air- and moisture-sensitive and show good solubility in low-polarity solvents (except **3**), such as benzene, toluene, and THF. Under a dry dinitrogen atmosphere, they can be kept for weeks without noticeable decomposition in the solid state and in solution. Dissolution of the complexes in THF develops red (for **1**−**4**) and orange (for **5** and **6**) solutions, and their absorption spectra in the UV−vis region are dominated by intense ligand-to-metal charge-transfer bands (Table S2 and Figures S1 and S2). The ^{1}H NMR spectra of **1**−**6** measured in C$_6$D$_6$ or THF-d_8 show well-resolved peaks in the range 0−8 ppm. The resonances of the carbene carbons in the ^{13}C NMR spectrum of **1** appears at ca. 200 ppm, and those of the cAAC complexes **2**, **4**, **5**, and **6** are 307.00, 307.00, 319.75, and 320.10 ppm, respectively. The well-resolved NMR spectra are indicative of their diamagnetic nature.

The molecular structures of **4**−**6** in solid states were established by X-ray diffraction studies. Figure 1 shows their structures, and Table 1 compiles the key distances and angles.

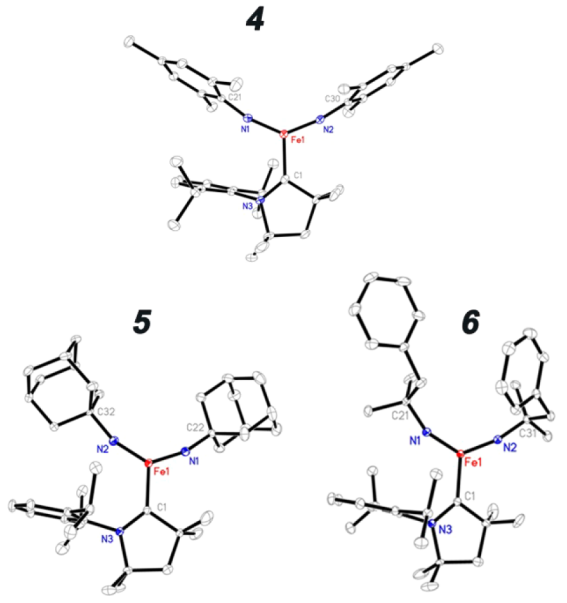

Figure 1. Molecular structures of **4**−**6**, showing 30% probability ellipsoids and the partial atom numbering schemes.

DOI: 10.1021/jacs.5b09579
J. Am. Chem. Soc. 2015, 137, 14196−14207

Table 1. Selected Distances (Å) and Angles (deg) of the Iron Imido Complexes from X-ray Crystal Structures

	1[a]	2[a]	4	5[b]	6	9
Fe−N(imido)	1.633(2)	1.636(2)	1.635(2)	1.612(2)	1.612(2)	1.708(2)
		1.635(2)	1.628(2)		1.616(2)	
Fe−C(carbene)	1.899(3)	1.905(4)	1.879(3)	1.867(2)	1.871(2)	2.086(3)
N(imido)−C(imido)	1.377(3)	1.371(2)	1.376(4)	1.455(8)	1.446(2)	1.352(4)
		1.376(2)	1.378(3)		1.443(2)	
N(imido)−Fe−N(imido)	141.0(2)	138.5(1)	134.5(2)	128.7(1)	127.9(1)	
N(imido)−Fe−C(carbene)	109.5(1)	112.8(1)	114.6(2)	115.7(1)	118.3(1)	
		108.0(1)	110.7(2)		113.9(1)	
Fe−N(imido)−C(imido)	166.5(2)	164.9(2)	166.4(2)	161.5(6)	156.5(2)	172.7(2)
		170.0(2)	169.1(2)		165.8(2)	
α[c]	26.9	33.8	10.4	9.0	8.4	

[a]Data from ref 19. [b]Data are the averages from two crystallographically independent molecules in the unit cell. [c]Dihedral angle between the N(imido)−Fe−N(imido) plane and the idealized carbene plane.

By analogy to **1** and **2**,[19] the iron centers in the structures of **4**−**6** exhibit a trigonal planar coordination geometry. The Fe−C(carbene) distances in **1**, **2**, and **4**−**6** are in the range 1.871(2)−1.905(4) Å, typical of low-spin iron-NHC compounds.[20] The Fe−N(imido) distances of the bisimido complexes (1.636(2)−1.612(2) Å) are shorter than that of Holland's three-coordinate iron(III) imido complex [(nacnac)Fe(NAd)] (1.67 Å)[9c] and comparable to those of the four-coordinate low-spin iron imido complexes.[8,10,13,14,17,18] Comparing the structural parameters of **1**, **2**, and **4**−**6** revealed that the Fe−N(imido) bonds of the arylimido complexes (**1**, **2**, and **4**) are slightly longer than those of the alkylimido compounds (**5** and **6**) and that the Fe−N(imido)−C(imido) alignments in the arylimido complexes, with the angles ranging between 170.0(2) and 164.9(2)°, are closer to linear than those of the alkylimido complexes (165.8(2)−156.5(2)°). These differences are likely due to electron delocalization within the arylimido fragments, as reflected by the short C(aryl)−N(imido) distances, which is absent in the alkylimido complexes.

The zero-field 80 K ^{57}Fe Mössbauer spectra of **3**−**6** were recorded. As representatives, the spectra of **4** and **6** are shown in Figure 2. Table 2 compiles the fitting isomer shifts (δ) and quadrupole splitting data ($|\Delta E_Q|$), including those of **1** and **2**. All the Mössbauer spectra consist of a single quadrupole doublet with negative isomer shift. The isomer shifts (δ = −0.29 to −0.52 mm/s) are apparently distinct from those of the three-coordinate iron(III) imido complex [(nacnac)Fe(NAd)] (0.47 mm/s)[9a] and iron(II) amide complex [(IPr)Fe(NHDipp)$_2$] (0.58 mm/s).[19] As compared with the reported iron(IV) species, these isomer shifts are negatively shifted from those of the low-spin iron(IV) imido complex [(pyrrol$_2$py)Fe^{IV}(NAd)] (−0.09 mm/s),[17] closer to those of the low-spin iron(IV) nitride complexes [{PhBP$_3$}Fe^{IV}(N)] (−0.34 mm/s)[21] and [(triscarbeneborate)Fe^{IV}(N)]$^+$ (−0.28 mm/s).[22] Within the series of three-coordinate iron(IV) imido complexes, a gradually decreasing trend of the δ value from NHC-iron-arylimido complexes to cAAC-iron-arylimido complexes and to cAAC-iron-alkylimido complexes in the order of **1** ≈ **3** > **2** ≈ **4** > **5** ≈ **6** can be identified. This trend should be related to the higher covalency of the Fe−C(cAAC) bond versus Fe−C(NHC) bond[23] and the stronger donating ability of alkylimido versus arylimido ligands. The structures and Mössbauer data are consistent with the low-spin iron(IV) nature of these three-coordinate bisimido complexes.

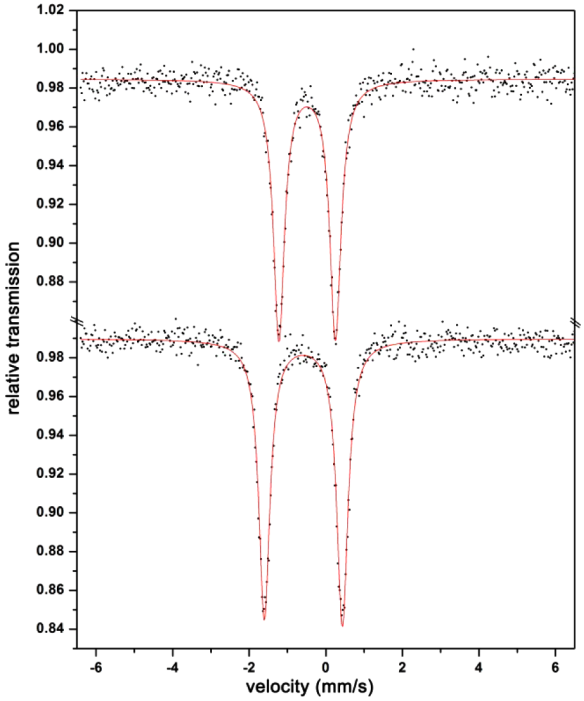

Figure 2. 80 K ^{57}Fe Mössbauer spectra of [(Me$_2$-cAAC)Fe(NMes)$_2$] (**4**, top) and [(Me$_2$-cAAC)Fe(NMe$_2$CH$_2$Ph)$_2$] (**6**, bottom). The data (dots) and best fit (solid line) are shown. The fitting parameters are listed in Table 2.

Table 2. ^{57}Fe Mössbauer Spectroscopic Data of **1**−**6**, **9**, and **10**

	δ, mm/s	$\lvert\Delta E_Q\rvert$, mm/s		δ, mm/s	$\lvert\Delta E_Q\rvert$, mm/s
1[a]	−0.32	1.89	**5**	−0.51	1.96
2[a]	−0.39	1.60	**6**	−0.52	2.04
3	−0.29	1.84	**9**	0.17	1.31
4	−0.44	1.47	**10**	0.16	1.34

[a]Data from ref 19.

Reactivity Study. As previously mentioned, while there are reports on the synthesis and characterization of iron(IV) imido compounds, their reactivity remained poorly understood. In view of the unique features of the iron(IV) bisimido compounds, the low coordination number of 3, and the high-

DOI: 10.1021/jacs.5b09579
J. Am. Chem. Soc. 2015, 137, 14196−14207

valent iron center, we next explored their representative reactivity using complex **1**.

Exploring the potential of **1** in promoting C−H bond activation revealed that **1** can neither react with toluene or 1,4-cyclohexadiene, despite the presence of relatively weak C(sp^3)−H bonds in these organic substrates, nor undergo intramolecular C−H bond amination like its cobalt analogue, [(IMes)Co(NDipp)$_2$].[24] However, **1** shows a unique reactivity of intramolecular alkane chain dehydrogenation. Heating a toluene solution of **1** at 100 °C for 24 h resulted in the formation of a light red solution, from which the iron(II) amide complex featuring an appended alkene side arm, [(IMes)Fe(NHDipp)(NHC$_6$H$_3$-2-Pr^i-6-CMe=CH$_2$)] (**7**), was isolated as red crystals in 64% yield (Scheme 2). The molecular structure

Scheme 2. C−H Bond Activation Reactivity of 1

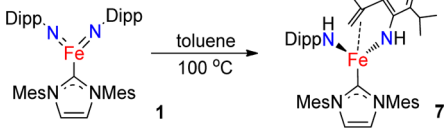

of **7**, established by an X-ray diffraction study, proved the presence of a C(olefin)−C(olefin) bond (1.416(10) Å) and weak iron(II)−olefin interactions (Figure 3). Moreover, ^{1}H

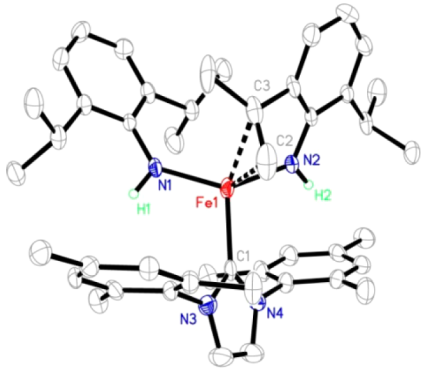

Figure 3. Molecular structure of **7**, showing 30% probability ellipsoids and the partial atom numbering scheme. Selected distances (Å): Fe(1)−C(1) 2.111(6), Fe(1)−N(1) 1.936(4), Fe(1)−N(2) 1.938(4), Fe(1)−C(2) 2.437(7), Fe(1)−C(3) 2.557(7), C(2)−C(3) 1.416(10).

NMR and GC-MS analyses of a hydrolyzed sample of **7** suggested the formation of H$_2$NDipp and H$_2$NC$_6$H$_3$-2-Pr^i-6-CMe=CH$_2$ in a nearly 1:1 ratio. The measured solution magnetic moment (μ_{eff} = 4.8(1) μ_B) and ^{57}Fe Mössbauer spectrum data (δ = 0.60 mm/s, $|\Delta E_Q|$ = 1.61 mm/s) of **7** corroborate its high-spin ground spin state S = 2.

Dehydrogenation of saturated hydrocarbon moieties by high-valent iron oxo species to form olefin functionalities is implicated in some enzymatic reactions, e.g., the introduction of double bonds into saturated fatty acids by desaturases.[25] Synthetic model reactions of this type, however, are rare. Que and co-workers had demonstrated that the in situ-generated iron(IV) oxo species (Tp^{Ph2})Fe(O)(O$_2$CPh) can dehydrogenate 9,10-dihydroanthracene, cyclohexene, and even cyclohexane, but not toluene or ethylbenzene.[26] Dehydrogenation of hydrocarbons by non-heme iron imido species was restricted to the reaction of 1,4-cyclohexadiene with [(nacnac)Fe(NAd)(NC$_5$H$_4$-p-Bu^t)][9d] and [(pyrrol$_2$)Fe(NC$_6$H$_4$-p-Bu^t)Cl][16a] and the reaction of 9,10-dihydroanthracene with Borovik's iron(IV) imido intermediate, formed from the interaction of K-[(^{t}BuNHC(O)NCH$_2$CH$_2$)$_2$(^{i}PrNC(O)CH$_2$)N)Fe] with p-tolyl azide.[27] In this regard, despite its intramolecular manner, the conversion of **1** to **7** is unique because it involves the oxidative dehydrogenation of an alkane chain by an isolable high-valent iron imido complex.

In contrast to the reluctance of **1** to undergo an intermolecular C−H activation reaction, **1** can active the Si−H bond in PhSiH$_3$ at room temperature to yield the high-spin iron(II) amido complex [(IMes)Fe(NHDipp)(NDipp-SiPhH$_2$)] (**8**) (Scheme 3). Complex **8** was characterized by

Scheme 3. Si−H Bond Activation Reactivity of 1

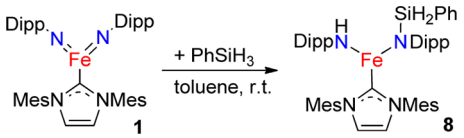

solution magnetic susceptibility measurement, ^{57}Fe Mössbauer spectroscopy, and X-ray crystallography. Figure 4 shows its

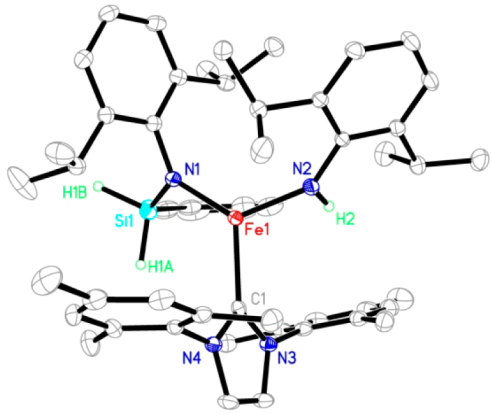

Figure 4. Molecular structure of **8**, showing 30% probability ellipsoids and the partial atom numbering scheme. Selected distances (Å) and angles (deg): Fe(1)−C(1) 2.121(2), Fe(1)−N(1) 1.937(2), Fe(1)−N(2) 1.924(2), N(1)−Si(1) 1.692(2), C(1)−Fe(1)−N(1) 122.76(8), C(1)−Fe(1)−N(2) 109.24(9), N(1)−Fe(1)−N(2) 125.39(8).

molecular structure. Si−H bond activation reactions are well-documented for early and middle transition metal imido complexes[28,29] but are rarely reported for late transition metal imido complexes. The known examples of the latter are restricted to the reaction of the iron(II) aminoimido compound [PhB(o-Pr$^i_2$PC$_6$H$_4$)$_2$FeNN(SiMe$_2$CH$_2$)$_2$] with PhSiH$_3$ to produce the iron(II) amido bridging hydrido complex [PhB(μ-H)(o-Pr$^i_2$PC$_6$H$_4$)$_2$FeN(SiH$_2$Ph)N(SiMe$_2$CH$_2$)$_2$][30] and the reactions of the two-coordinate cobalt(II) imido complex [(IPr)Co(NDmp)] with PhSiH$_3$ and Ph$_2$SiH$_2$ to form cobalt(II) amido complexes.[31] Unlike these non-redox reactions, the reaction of **1** with PhSiH$_3$ resulted in the reduction of the iron(IV) center to iron(II), reflecting the oxidizing power of the iron(IV) imido species.

Examining the reactions of **1** with polar unsaturated organic molecules revealed its [2+2]-addition reactions with hetero-cumulenes, which enabled the preparation of novel open-shell formal iron(IV) monoimido complexes. The reaction of **1** with

DOI: 10.1021/jacs.5b09579
J. Am. Chem. Soc. 2015, 137, 14196−14207

1 equiv of PhNCNPh or *p*-Pr^{i}C$_6$H$_4$NCO in toluene proceeded quickly at room temperature. From the resultant brown solutions, the red paramagnetic formal iron(IV) monoimido complexes [(IMes)Fe(NDipp)(N(Dipp)C(NPh)(=NPh))] (**9**) and [(IMes)Fe(NDipp)(N(Dipp)C(O)N(*p*-Pr^{i}C$_6$H$_4$))] (**10**) were isolated in moderate yields (Scheme 4). Complexes

Scheme 4. [2+2]-Addition Reactions of 1 with Heterocumulenes

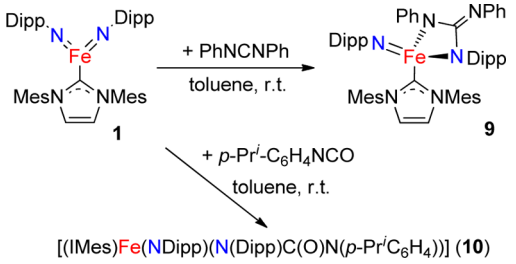

9 and **10** were characterized by ^{1}H NMR, solution magnetic susceptibility measurements, Mössbauer spectroscopy, and elemental analyses. In addition, the molecular structure of **9** was unequivocally established by an X-ray diffraction study. While attempts to grow single crystals of **10** suitable for X-ray diffraction were unsuccessful, the isolation of the urea DippHNC(O)NH(*p*-Pr^{i}C$_6$H$_4$) from the quenching experiment of **10**, along with the close resemblance of the paramagnetic ^{1}H NMR spectrum and the Mössbauer data (Table 2) of **10** with those of **9**, suggest its identity as a four-coordinate formal iron(IV) monoimido complex bearing an *N*,*N*- or *N*,*O*-urinate chelate. Notably, although precedents of [2+2]-addition reactions of imido complexes with unsaturated organic substrates are well-known for early and middle transition metal imido complexes,[28,32] such a reactivity is rarely observed on late transition metal imido complexes, namely [Cp*Ir(NBu^t)][32] and [(Bu$^t_2$PCH$_2$CH$_2$PBu$^t_2$)Ni(NR)].[34]

As shown in Figure 5, the structure of **9** contains a guanidinato ligand that chelates to the iron center with Fe–N distances of 1.944(2) and 1.927(3) Å. The intact imido moiety

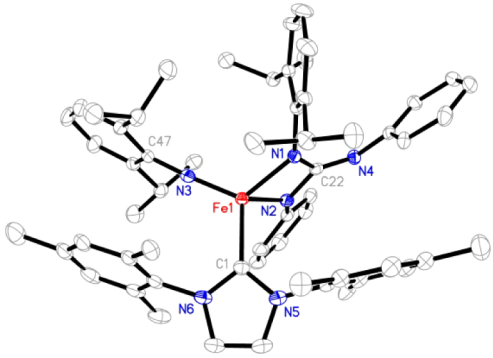

Figure 5. Molecular structure of **9**, showing 30% probability ellipsoids and the partial atom numbering scheme. Selected distances (Å) and angles (deg): Fe(1)–C(1) 2.086(3), Fe(1)–N(1) 1.944(2), Fe(1)–N(2) 1.927(3), Fe(1)–N(3) 1.708(2), C(22)–N(1) 1.395(4), C(22)–N(2) 1.388(3), C(22)–N(4) 1.283(4), C(1)–Fe(1)–N(1) 120.48(11), C(1)–Fe(1)–N(2) 104.37(11), C(1)–Fe(1)–N(3) 113.21(12), N(1)–Fe(1)–N(2) 68.41(10), N(1)–Fe(1)–N(3) 119.12(10), N(2)–Fe(1)–N(3) 123.42(11), Fe(1)–N(3)–C(47) 172.7(2).

has an Fe–N(imido)–C(imido) angle of 172.7(2)° and Fe–N(imido) distance of 1.708(2) Å. This bond distance is longer than those of the aforementioned three- and four-coordinate low-spin iron(IV) imido complexes (1.65 and 1.61 Å)[13,14,19] and closer to those in the four-coordinate open-shell species [(PDI^{Dipp})Fe(NDipp)] (1.71 Å)[11a] and [(pyrrol$_2$)Fe(NC$_6$H$_4$-*p*-Bu^t)Cl] (1.77 Å).[16a] The Fe–C(carbene) bond in **9** (2.086(3) Å) is also much longer than its congener in **1** (1.899(3) Å).[19] The Mössbauer spectrum of **9** contains a single quadrupole doublet with the fitting isomer shift δ = 0.17 mm/s and quadrupole splitting $|\Delta E_Q|$ = 1.31 mm/s. The isomer shift is closer to that of the open-shell species [(pyrrol$_2$)Fe(NC$_6$H$_4$-*p*-Bu^t)Cl] (0.29 mm/s),[16a] rather than the negative isomer shifts of the aforementioned low-spin iron(IV) imido and nitrido complexes.[17,19,21,22] These characterization data, in addition to its measured solution magnetic moment (4.0(1) μ_B in C$_6$D$_6$) which locates it between the spin-only values of S = 1 and S = 2 ions (2.83 and 4.90 μ_B, respectively), suggest the open-shell nature of this iron imido species.[35]

In addition to the previously mentioned reactions, **1** can also undergo group-transfer reactions to CO and Bu^{t}NC at room temperature to produce DippNCO and DippNCNBu^t, respectively. NMR quantifications on the organic products proved the transfer of both imido moieties of **1** in these reactions. An iron-containing product, [(IMes)Fe(CO)$_4$],[36] has been isolated in the reaction with CO. Attempts to isolate the iron(0) isocyanide product (IMes)Fe(CNBu^t)$_4$ proved futile, probably due to its instability.[37] As the group-transfer reactions hint at the electrophilic nature of the imido moieties in **1**, the reactions of **1** with a series of alkenes, e.g., ethylene, styrene, phenylallene, and dimethyl fumarate, were examined, with the aim to achieve the diamination of alkenes.[38] Unfortunately, none of these reactions occurred at either room temperature or 60 °C. Complex **1** is also inert toward the alkynes 3,3-dimethyl-1-butyne and phenylacetylene. These results indicate the weak electrophilic nature of the NDipp groups in **1**.

Theoretical Studies. The E–H σ-bond (E = C, Si) activation reactions discussed above resulted in the conversions of the iron(IV) bisimido complex to iron(II) bisamide complexes and different spin states of the products versus the starting materials ($S_{reactant}$ = 0 and $S_{product}$ = 2). To shed light on their reaction mechanisms, DFT calculations employing TPSS functional were performed.[39]

Calculations on [(IMes)Fe(NDipp)$_2$] (**1**) indicated that the low-spin (S = 0) state is the ground state, and it lies 2.9 and 11.1 kcal/mol below the triplet (S = 1) and quintet (S = 2) states in Gibbs free energy, respectively. Table S3 lists the key structural parameters of the optimized structures at the three spin states. Among them, the singlet-state structure has bond distances and angles around the FeN$_2$C core more similar to those obtained from X-ray diffractions study and has calculated ^{57}Fe Mössbauer parameters (δ = −0.49 mm/s, ΔE_Q = −2.17 mm/s) comparable to the experimental data (δ = −0.32 mm/s, $|\Delta E_Q|$ = 1.89 mm/s).

Considering the current unavailability of a theoretical description of the electronic structure for a three-coordinate iron(IV) bisimido complex in the literature, here we first give a general picture of the electronic configurations and bonding of the singlet (S = 0) and triplet (S = 1) states of **1**. As shown in Figure 6, the interaction of the five 3d(Fe) orbitals and the five N/C ligand orbitals dominates the electronic structure of **1**. Owing to its trigonal planar coordination geometry, the Fe d_{xy}/$d_{x^2-y^2}$ atomic orbitals in the FeN$_2$C plane have strong bonding

DOI: 10.1021/jacs.5b09579
J. Am. Chem. Soc. 2015, 137, 14196–14207

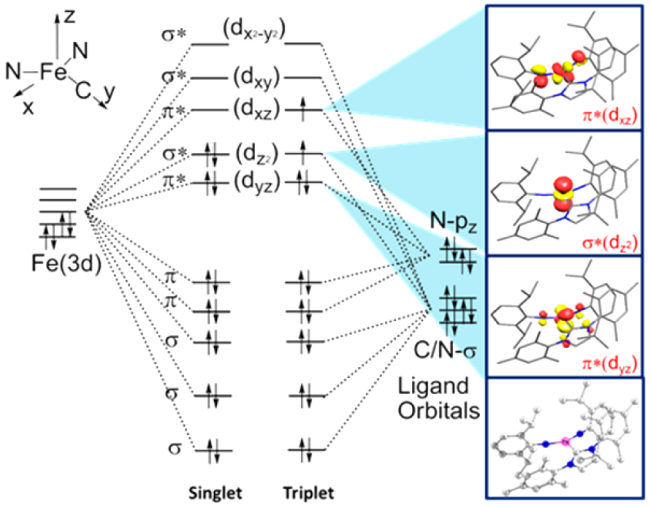

Figure 6. Electronic configurations of ground singlet and excited triplet states based on key orbital interactions between the central iron atom and its ligands for **1**.

and antibonding interactions with the σ-type ligand orbitals, resulting in the low-lying σ-bonding and high-lying σ^* antibonding molecular orbitals (MOs). On the other hand, due to the orbital shape, the overlap between Fe d_{z^2} and σ-type ligand orbitals is much weaker, leaving the resulting $\sigma^*(d_{z^2})$ MO as a frontier molecular orbital (FMO) doubly and singly occupied in singlet and triplet states, respectively. In addition to these, the p_z orbitals on two imido N atoms perpendicular to the FeN_2C plane bear some weaker bonding/antibonding interactions with the d_{yz} and d_{xz} orbitals of the Fe center, producing MOs $\pi^*(d_{yz})/\pi^*(d_{xz})$. These two MOs are doubly occupied and nonoccupied, respectively, in the singlet state and doubly/singly occupied in the excited triplet state. Hence, the singlet state of **1** has a closed-shell electronic structure, in which $\sigma^*(d_{z^2})$ and $\pi^*(d_{xz})$ are highest occupied and lowest unoccupied molecular orbitals (HOMO and LUMO), respectively. From a closed-shell singlet state, a HOMO–LUMO excitation from $\sigma^*(d_{z^2})$ to $\pi^*(d_{xz})$ makes both FMOs singly occupied, thus generating a triplet-state configuration with weak Fe–N bonds and enhanced reactivity (*vide infra*). Importantly, the components and direction of HOMO and LUMO imply that substrates should approach the Fe–N moieties from the out-of-plane directions.

Ideally, **1** could facilitate E–H bond (E = C, Si) activation in three manners: synergistic interaction, hydrogen atom abstraction (HAA), and 1,2-addition (Chart 1).[40,41] We initially examined the synergistic interaction mode. Despite its concise manner, the synergistic pathway for the C–H activation reaction of **1** (the conversion of **1** to **7**) via the transition state **A** (Chart 1) has a very high activation energy (54.5 kcal/mol, see Figure S34 for details), which renders it energetically disfavored. As for the Si–H bond activation, no viable transition state, in the form of **A′** in Chart 1, linking the reactant and product could be located, implying the necessity of an intermediate to intervene in the reaction. Subsequently, the other two reaction pathways, HAA and 1,2-addition, were examined, which revealed that HAA and 1,2-addition mechanisms at the triplet energy surfaces for the C–H and Si–H bond activation reactions of **1** are the energetically more favorable pathways, respectively.

Chart 1. Possible Interaction Modes of Fe-NDipp in 1 with the E–H Bonds

	Synergestic Interaction	H-Abstraction[a]	1,2-Addition[a,b]
C-H Activation	A	B	C
Si-H Activation	A′	B′	C′

[a]For simplicity, only one of the possible interactions for each mode is depicted. [b]The interaction of two hydrogen atoms with one Fe–N(imido) fragment is denoted as a 1,2-addition activation mode for the E–H activation reaction.

The most favorable DFT-calculated reaction pathway for the intramolecular alkane dehydrogenation of **1** is depicted in Figure 7.[42] First, one imido N atom of **1** abstracts a benzylic

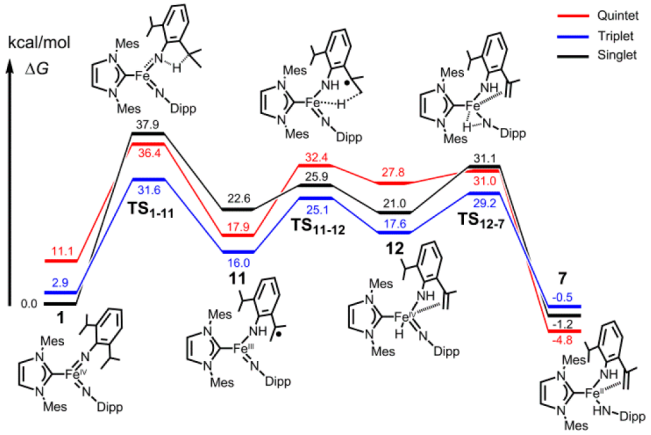

Figure 7. DFT-calculated reaction profile of the dehydrogenative C–H bond activation reaction of **1**.

hydrogen atom from a Dipp group through transition state $\mathbf{TS_{1-11}}$, resulting in intermediate **11** bearing a benzylic radical. Then via $\mathbf{TS_{11-12}}$, one methyl hydrogen atom adjacent to the benzylic radical migrates to the Fe center, leading to the Fe(IV)–H intermediate **12** with the concurrent formation of a C=C bond on the Dipp group. **12** then undergoes a migratory insertion reaction to produce the final product **7**. The net reaction has a small thermodynamic driving force of ca. 5 kcal/mol, and the rate-limiting step of the mechanism is the benzylic HAA by the bisimido complex (**1** to **11**).

The transition states of this step ($\mathbf{TS_{1-11}}$) at singlet, triplet, and quintet states lay 37.9, 31.6, and 36.4 kcal/mol, respectively, above the singlet ground state of **1**, suggesting that the triplet-state transition state could be reached more easily. This barrier is in line with the experimental high reaction temperature and relatively slow reaction rate. In comparison, the calculated barrier is much higher than the experimentally measured barrier of 20 kcal/mol for the intramolecular HAA of the iron(III) imido species (nacnac)Fe(NAd)(NC_5H_4-*p*-Bu^t) reported by Cundari and Holland[9c] and the calculated barrier of 17 kcal/mol for the intermolecular HAA of the iron(IV) imido

DOI: 10.1021/jacs.5b09579
J. Am. Chem. Soc. 2015, 137, 14196–14207

species $[(N4Py)Fe(NTs)]^{2+}$ with 1,4-cyclohexadiene reported by de Visser et al.[41h] The high barrier of the current system might be related to the nonlinear N(imido)···H···C(benzyl) alignment in the transition state $\mathbf{TS_{1-11}}$ (Figure 8), as HAA

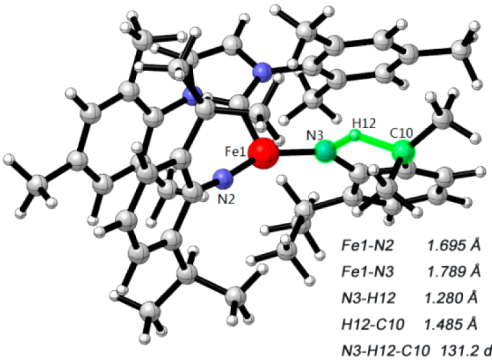

Figure 8. Optimized geometry of $\mathbf{TS_{1-11}}$ at the triplet state.

usually takes place in a linear A··H···B transition state.[43] Importantly, except for the reactant **1** and the product **7**, the whole middle part the triplet reaction profile is lower in energy than both the singlet and quintet states, which implies that spin transitions are necessary during the reaction and multi-state reactivity is quite possible.[44]

The DFT-calculated most favorable pathway for the reaction of **1** with $PhSiH_3$ is depicted in Figure 9.[45] First, one imido

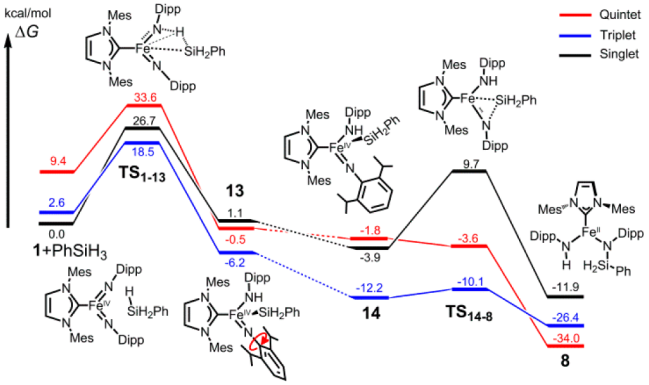

Figure 9. DFT-calculated reaction profile of the Si−H bond activation reaction of **1** with $PhSiH_3$.

group in **1** interacts with one Si−H bond in $PhSiH_3$ via the $[2\pi+2\sigma]$-addition transition state $\mathbf{TS_{1-13}}$ to generate Fe(IV)−silyl intermediate **13** (Figure 10). **13** then rotates one of the Dipp groups, leading to the intermediate **14**. A further migratory insertion reaction from **14** via $\mathbf{TS_{14-8}}$ then produces the final product **8**. The reaction has a thermodynamic driving force of more than 30 kcal/mol, which is much larger than that of the above dehydrogenation reaction of **1**. Interestingly, similar to the dehydrogenation reaction, the triplet state here is also the lowest energy profile linking the reactant and product.

Despite the distinct mechanisms of the E−H (E = C, Si) activation reactions, two common features are still noticeable. First, the structures of the transition states, $\mathbf{TS_{1-11}}$ and $\mathbf{TS_{1-13}}$, indicate that the E−H bond activation reactions occur in the out-of-plane direction (relative to the FeN_2C plane) of the iron imido complex, which is in agreement with the aforementioned electronic structure and FMO analyses on **1**. Second, in

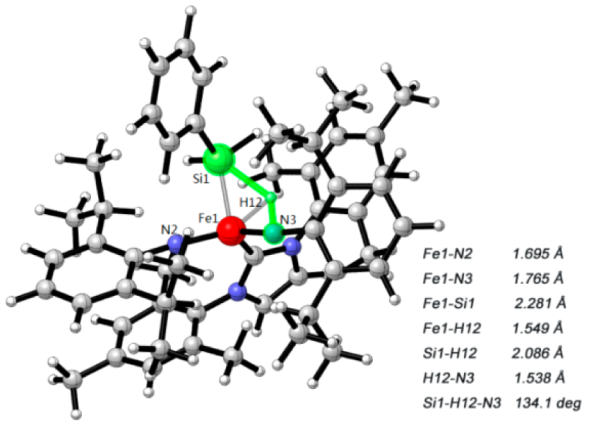

Figure 10. Optimized geometry of $\mathbf{TS_{1-13}}$ at the triplet state.

addition to the imido N atoms, the Fe center is also involved in the bond-cleaving and -forming processes, as reflected by the formation and transformation of the iron(IV) hydride species **12** and iron(IV) silyl intermediate **13**. This is in marked contrast to the reactions of iron oxo and iron imido systems with high coordination numbers, wherein there is no direct involvement by the metal center,[43b,46] signifying the unique reactivity of the low-coordinate iron(IV) imido complex.

CONCLUSIONS

We have performed a systematic study on the synthesis, characterization, and reactivity of the three-coordinate iron(IV) bisimido complexes with aminocarbene ligation $[(L)Fe(NR)_2]$ (L = cyclic aminocarbene; R = aryl, alkyl).

Exploring the reactions of three-coordinate iron(0)−alkene complexes $(L)Fe(\eta^2{:}\eta^2\text{-dvtms})$ with bulky organic azides led to the preparation of the arylimidoiron(IV) complexes $[(NHC)Fe(NDipp)_2]$ (NHC = Mes, IPr) and $[(Me_2\text{-cAAC})Fe(NAr)_2]$ (Ar = Dipp, Mes) and also the alkylimido complexes $[(Me_2\text{-cAAC})Fe(NR)_2]$ (R = Ad, CMe_2CH_2Ph). Characterization data obtained from NMR spectroscopy, X-ray crystal structure determination, and ^{57}Fe Mössbauer spectroscopy, in combination with DFT theoretical calculations, collectively indicate the low-spin nature of these three-coordinate iron(IV) bisimido complexes.

The reactivity of the iron(IV) imido complexes was explored with the reactions of $[(IMes)Fe(NDipp)_2]$ as the representatives. Investigating the reactions of $[(IMes)Fe(NDipp)_2]$ with unsaturated organic substrates disclosed its [2+2]-addition reactions with PhNCNPh and $p\text{-Pr}^iC_6H_4NCO$ to form the open-shell formal iron(IV) monoimido species $[(IMes)Fe(NDipp)(N(Dipp)C(NPh)(=NPh))]$ and $[(IMes)Fe(NDipp)(N(Dipp)C(O)N(p\text{-Pr}^iC_6H_4))]$, respectively. In addition, the iron(IV) bisimido complex can perform [NDipp]-transfer reactions to CO and Bu^tNC. $[(IMes)Fe(NDipp)_2]$ can also activate E−H (E = C, Si) σ-bonds. When heated, it converted to the iron(II) complex bearing an alkene side arm, $[(IMes)Fe(NHDipp)(NHC_6H_3\text{-}2\text{-Pr}^i\text{-}6\text{-CMe}{=}CH_2)]$. The conversion is reminiscent of the alkane desaturation reactivity of high-valent iron oxo species proposed in enzymatic and biomimetic model reactions. $[(IMes)Fe(NDipp)_2]$ can react with $PhSiH_3$ to produce the iron(II) amido complex $[(IMes)Fe(NHDipp)(NDippSiPhH_2)]$.

DFT calculations on the mechanism of C−H and Si−H activation reactions indicated that (i) the C−H bond activation reaction might proceed via a HAA mechanism and the Si−H

DOI: 10.1021/jacs.5b09579
J. Am. Chem. Soc. 2015, 137, 14196−14207

bond activation reaction via a $[2\pi+2\sigma]$-addition mechanism; (ii) organometallic intermediates, iron(IV) hydride and iron-(IV) silyl species, are important intermediates in the C−H and Si−H activation reactions; and (iii) both reactions have a multi-state reactivity and the bond-forming and -cleavage steps on the triplet potential energy surface have the lowest energy profiles. The co-occurrence of the HAA and $[2\pi+2\sigma]$-addition reactions signifies the uniqueness of the iron imido complex among the reported transition metal imido compounds, which should benefit from its readily accessibility of the triplet state, as well as the low-coordinate and high-valent nature.

EXPERIMENTAL SECTION

General Procedures. All experiments were performed either under an atmosphere of dry dinitrogen with the rigid exclusion of air and moisture using standard Schlenk techniques or in a glovebox. Organic solvents were dried with a solvent purification system (Innovative Technology) and bubbled with dry N_2 gas prior to use. [(IMes)Fe(η^2:η^2-dvtms)],[19] [(Me_2-cAAC)Fe(η^2:η^2-dvtms)],[19] 2,5-di-(2′,6′-diisopropylphenyl)imidazol-1-ylidene (IPr),[47] 2,6-diisopropyl-phenyl azide ($DippN_3$),[48] 2,4,6-trimethylphenyl azide ($MesN_3$),[48] 1-adamantyl azide (AdN_3),[49] 2-azido-2-methyl-1-phenylpropane ($PhCH_2Me_2CN_3$),[50] and 1,3-diphenyl carbodiimide[51] were synthesized according to literature procedures. All other chemicals were purchased from either Strem or J&K Chemical Co. and used as received unless otherwise noted. ^{1}H NMR and ^{13}C NMR spectra were recorded on Agilent 300, 400, and 600 MHz spectrometers. All chemical shifts are reported in units of ppm with reference to the residual protons of the deuterated solvents for proton and carbon chemical shifts. Elemental analysis was performed by the Analytical Laboratory of Shanghai Institute of Organic Chemistry (CAS). Magnetic moments were measured by the method originally described by Evans with stock and experimental solutions containing a known amount of a $(CH_3)_3SiOSi(CH_3)_3$ standard.[52] Absorption spectra were recorded with a Shimadzu UV-3600 UV-vis-NIR spectrophotometer. IR spectra were recorded with a Nicolet Avatar 330 FT-IR spectrophotometer. Melting points were measured with samples sealed in thin-walled glass capillaries, and the nature of the samples was re-checked by ^{1}H NMR after the measurements.

X-ray Structure Determination. Diffraction-quality crystals were obtained from recrystallizations in Et_2O (**4**, **6**, and **7**), *n*-hexane (**5**), and Et_2O/*n*-hexane (**9**). Crystals were coated with Paratone-*N* oil and mounted on a Bruker Apex CCD-based diffractometer equipped with an Oxford low-temperature apparatus. Cell parameters were retrieved with SMART software and refined using SAINT software on all reflections. Data integration was performed with SAINT, which corrects for Lorentz polarization and decay. Absorption corrections were applied using SADABS.[53] Space groups were assigned unambiguously by analysis of symmetry and systematic absences determined by XPREP. All structures were solved and refined using SHELXTL.[54] Metal and first-coordination-sphere atoms were located from direct-methods E-maps. Non-hydrogen atoms found in alternating difference Fourier synthesis and least-squares refinement cycles and during final cycles were refined anisotropically. Table S1 summarizes the crystal data and data collection and refinement for the complexes.

^{57}Fe Mössbauer Spectroscopy. All ^{57}Fe Mössbauer spectroscopy was run on non-enriched solid samples of the as-isolated complexes. Each sample was loaded into a Delrin Mössbauer sample cup for measurements and loaded under liquid nitrogen. Low-temperature ^{57}Fe Mössbauer measurements were performed using a SeeCo MS4 Mössbauer spectrometer integrated with a Janis SVT-400T He/N_2 cryostat for measurements at 80 K. Isomer shifts were determined relative to α-Fe at 298 K. All Mössbauer spectra were fit using the program WMoss (SeeCo).

Preparation of [(IPr)Fe(η^2:η^2-dvtms)]. This complex was prepared via procedures similar to those used for [(IMes)Fe(dvtms)]. To a stirring THF (50 mL) solution of IPr (1.01 g, 2.6 mmol) were added $FeCl_2$ (330 mg, 2.6 mmol) and dvtms (540 mg, 2.6 mmol) at room temperature. After the mixture was stirred for 30 min, KC_8 (770 mg, 5.7 mmol) was added and stirring was continued for a further 48 h, during which the color changed to blue gradually. The mixture was then filtered through Celite and concentrated under vacuum to afford a blue residue that was washed with *n*-hexane (10 mL) and dried under vacuum to give [(IPr)Fe(dvtms)] as a blue powder (1.24 g, 76%), mp = 202−204 °C. ^{1}H NMR (400 MHz, C_6D_6, 295 K): δ (ppm) 1.62 (br), 1.12 (br), −0.30 (br), −3.04 (br), −10.89 (br), −17.44 (br). Anal. Calcd for $C_{35}H_{54}FeN_2OSi_2$: C, 66.64; H, 8.63; N, 4.44. Found: C, 66.22; H, 8.82; N, 4.46. Magnetic susceptibility (C_6D_6, 294 K): μ_{eff} = 3.6(1) μ_B. Absorption spectrum (THF): λ_{max}, nm (ε, M^{-1} cm^{-1}) = 380 (2600), 597 (130), 748 (190). IR (KBr, cm^{-1}): ν = 3086 (m), 2960 (s), 2868 (m), 1679 (s), 1471 (m), 1422 (m), 1383 (w), 1361 (w), 1255 (m), 1132 (w), 1060 (m), 1009 (m), 923 (m), 839 (m), 778 (m), 689 (w).

Preparation of [(IPr)Fe(NDipp)$_2$] (3). To a blue solution of [(IPr)Fe(η^2:η^2-dvtms)] (249 mg, 0.39 mmol) in toluene (5 mL) was added $DippN_3$ (162 mg, 0.80 mmol) at room temperature. The color of the solution changed from blue to red immediately, and bubbles were released vigorously. The reaction mixture was stirred at room temperature for 2 h. All the volatiles were then removed under a vacuum to leave a red solid. The red residue was extracted with Et_2O/THF (1:1, 5 mL), and the solution was filtered to leave a clear red solution. Slow evaporation of the solvent at room temperature afforded **3** as red crystals (215 mg, 69%), mp = 170−172 °C (decomposed). ^{1}H NMR (400 MHz, THF-d_8, 295 K): δ (ppm) 8.07 (s, 2H, C*H*═C*H*), 7.72 (t, J = 7.7 Hz, 2H, *p*-C_6H_3), 7.22 (t, J = 7.7 Hz, 2H, *p*-C_6H_3), 7.02 (d, J = 7.7 Hz, 4H, *m*-C_6H_3), 6.53 (d, J = 7.7 Hz, 4H, *m*-C_6H_3), 2.98−2.83 (m, 4H, C*H*$(CH_3)_2$), 2.72 (m, 4H, C*H*$(CH_3)_2$), 1.16 (d, J = 6.6 Hz, 12H, CH$(CH_3)_2$), 0.97 (d, J = 5.8 Hz, 24H, CH$(CH_3)_2$), 0.84 (d, J = 6.3 Hz, 12H, CH$(CH_3)_2$). ^{13}C NMR (101 MHz, THF-d_8, 295 K): δ (ppm) 147.53, 140.06, 139.47, 134.83, 131.15, 129.44, 125.08, 124.71, 118.75, 30.86, 30.47, 26.43, 24.38, 23.45. No signal for carbene carbon was observed. Anal. Calcd for $C_{51}H_{70}FeN_4$: C, 77.05; H, 8.88; N, 7.05. Found: C, 76.93; H, 8.71; N, 6.96. Absorption spectrum (THF): λ_{max}, nm (ε, M^{-1} cm^{-1}) = 290 (8300), 362 (1300), 746 (210). IR (KBr, cm^{-1}): ν = 3050 (w), 2962 (s), 2868 (m), 1699 (w), 1577 (w), 1466 (s), 1409 (w), 1394 (w), 1379 (w), 1364 (w), 1318 (m), 1301 (m), 1280 (m), 1180 (w), 1104 (w), 1094 (w), 1072 (w), 1060 (w), 1045 (w), 986 (w), 967 (w), 934 (w), 799 (m), 757 (s), 740 (m), 680 (w), 583 (w).

Preparation of [(Me_2-cAAC)Fe(NMes)$_2$] (4). To a green solution of [(Me_2-cAAC)Fe(η^2:η^2-dvtms)] (217 mg, 0.41 mmol) in toluene (10 mL) was added $MesN_3$ (136 mg, 0.84 mmol) at room temperature. The color of the solution changed from green to red immediately, and bubbles were released vigorously. The reaction mixture was stirred at room temperature for 2 h. All the volatiles were then removed under a vacuum to leave a red solid. The red residue was extracted with Et_2O (3 mL), and the solution was filtered. Slow evaporation of the solvent at room temperature afforded **4** as red crystals suitable for X-ray crystallography (147 mg, 59%), mp = 138−141 °C (decomposed). ^{1}H NMR (400 MHz, C_6D_6, 295 K): δ (ppm) 7.05 (t, J = 7.7 Hz, 1H, *p*-C_6H_3), 6.88 (d, J = 7.7 Hz, 2H, *m*-C_6H_3), 6.55 (s, 4H, *m*-C_6H_2), 3.49−3.37 (m, 2H, C*H*$(CH_3)_2$), 2.26 (s, 2H, CH_2), 2.11 (s, 12H, CH_3), 1.77 (s, 6H, CH_3), 1.36 (s, 6H, CH_3), 1.21 (d, J = 6.7 Hz, 6H, CH$(CH_3)_2$), 1.19 (s, 6H, CH_3), 0.92 (d, J = 6.7 Hz, 6H, CH$(CH_3)_2$). ^{13}C NMR (101 MHz, C_6D_6, 295 K): δ (ppm) 307.00 ($C_{carbene}$), 161.04, 146.39, 139.34, 131.82, 129.35, 129.26, 127.40, 124.54, 78.07, 59.41, 53.06, 32.68, 29.75, 28.92, 26.75, 24.35, 21.75, 20.75. Anal. Calcd for $C_{38}H_{53}FeN_3$: C, 75.10; H, 8.79; N, 6.91. Found: C, 74.89; H, 9.04; N, 6.94. Absorption spectrum (THF): λ_{max}, nm (ε, M^{-1} cm^{-1}) = 300 (11400), 332 (10400), 428 (6500), 889 (280). IR (KBr, cm^{-1}): ν = 2967 (s), 2923 (s), 2867 (m), 1688 (s), 1600 (m), 1491 (m), 1467 (m), 1444 (m), 1387 (m), 1367 (m), 1347 (m), 1303 (w), 1291 (w), 1228 (w), 1190 (w), 1174 (w), 1126 (w), 984 (w), 851 (m), 803 (m), 751 (w), 562 (w).

Preparation of [(Me_2-cAAC)Fe(NAd)$_2$] (5). To a green solution of [(Me_2-cAAC)Fe(η^2:η^2-dvtms)] (210 mg, 0.40 mmol) in Et_2O (10 mL) was added AdN_3 (144 mg, 0.81 mmol) at room temperature. The

DOI: 10.1021/jacs.5b09579
J. Am. Chem. Soc. 2015, 137, 14196−14207

reaction mixture was stirred at room temperature for 12 h, during which time the color of solution changed from green to brown gradually. Removal of the solvent under a vacuum afforded a brown solid, which was redissolved in *n*-hexane (3 mL) and filtered. Recrystallization of the crude product from the *n*-hexane solution at −35 °C afforded **5** as brown crystals suitable for X-ray crystallography (113 mg, 44%), mp = 166−170 °C (decomposed). ^{1}H NMR (400 MHz, C_6D_6, 295 K): δ (ppm) 7.12−7.06 (m, 1H, *p*-C_6H_3), 6.97 (d, J = 7.7 Hz, 2H, *m*-C_6H_3), 3.43−3.30 (m, 2H, $CH(CH_3)_2$), 2.24 (s, 2H, CH_2), 2.11 (br, 12H, CH_2 on adamantyl), 1.95 (br, 6H, CH on adamantyl), 1.65 (d, J = 12.0 Hz, 6H, CH_2 on adamantyl), 1.56 (d, J = 12.0 Hz, 6H, CH_2 on adamantyl), 1.50 (s, 6H, CH_3), 1.32 (s, 6H, CH_3), 1.30 (d, J = 6.8 Hz, 6H, $CH(CH_3)_2$), 1.25 (d, J = 6.8 Hz, 6H, $CH(CH_3)_2$). ^{13}C NMR (101 MHz, C_6D_6, 295 K): δ (ppm) 319.75 ($C_{carbene}$), 146.28, 139.50, 127.50, 124.69, 77.38, 70.71, 56.41, 52.42, 44.41, 36.44, 34.98, 29.89, 29.86, 28.99, 28.82, 23.73. Anal. Calcd for $C_{40}H_{61}FeN_3$: C, 75.09; H, 9.61; N, 6.57. Found: C, 74.44; H, 9.80; N, 6.40. Absorption spectrum (THF): λ_{max}, nm (ε, M^{-1} cm^{-1}) = 411 (5900), 540 (1300), 724 (420). IR (KBr, cm^{-1}): ν = 2967 (s), 2905 (s), 2848 (s), 1691 (s), 1467 (m), 1450 (m), 1388 (m), 1367 (m), 1296 (w), 1252 (w), 1225 (w), 1149 (w), 1094 (w), 1051 (w), 799 (w), 750 (w), 591 (w).

Preparation of [(Me_2-cAAC)Fe($NCMe_2CH_2Ph$)$_2$] (6). To a green solution of [(Me_2-cAAC)Fe(η^2:η^2-dvtms)] (158 mg, 0.30 mmol) in Et_2O (10 mL) was added $PhCH_2Me_2CN_3$ (108 mg, 0.62 mmol) at room temperature. The reaction mixture was stirred at room temperature for 12 h, during which time the color of solution changed from green to brown gradually. Removal of the solvent under vacuum afforded a brown solid that was extracted with Et_2O (3 mL) and filtered. Slow evaporation of the solvent at room temperature afforded **6** as brown crystals suitable for X-ray crystallography (77 mg, 40%), mp = 169−172 °C (decomposed). ^{1}H NMR (400 MHz, C_6D_6, 295 K): δ (ppm) 7.31−7.29 (m, 4H, aryl CH), 7.18−7.14 (m, 4H, aryl CH), 7.10−7.05 (m, 2H, aryl CH), 7.05−6.93 (m, 3H, aryl CH), 3.36 (m, 2H, $CH(CH_3)_2$), 3.03 (br, 4H, CH_2Ph), 2.19 (s, 2H, CH_2), 1.45−1.18 (m, 36H, CH_3). ^{13}C NMR (101 MHz, C_6D_6, 295 K): δ (ppm) 320.10 ($C_{carbene}$), 146.25, 139.33, 138.88, 130.98, 127.85, 127.56, 125.88, 124.73, 77.75, 72.87, 56.90, 52.41, 48.81, 34.66, 29.82, 28.85, 28.56, 27.91, 23.66. Anal. Calcd for $C_{40}H_{57}FeN_3$: C, 75.57; H, 9.04; N, 6.61. Found: C, 75.25; H, 9.02; N, 6.53. Absorption spectrum (THF): λ_{max}, nm (ε, M^{-1} cm^{-1}) = 413 (7100), 533 (1400), 728 (390). IR (KBr, cm^{-1}): ν = 2967 (m), 2929 (m), 2867 (m), 1679 (s), 1602 (w), 1491 (w), 1467 (m), 1453 (m), 1391 (m), 1368 (m), 1323 (w), 1223 (w), 1148 (w), 1050 (w), 802 (w), 752 (w), 725 (w), 702 (m), 592 (w).

Decomposition of 1 at 100 °C. A toluene solution (5 mL) of **1** (201 mg, 0.28 mmol) was heated at 100 °C for 24 h, and the color of the solution changed from dark red to bright red gradually. Then, the solution was cooled to room temperature. Removal of the solvent under vacuum afforded a red solid. The solid residue was extracted with Et_2O (10 mL), and the solution was filtered. Slow evaporation of the solvent at room temperature afforded [(IMes)Fe(NHDipp)-(NHC_6H_3-2-Pr^i-6-CMe=CH_2)] (**7**) as red crystals suitable for X-ray crystallography (129 mg, 64%). ^{1}H NMR (400 MHz, C_6D_6, 294 K): δ (ppm) 58.39 (br), 57.80 (br), 46.67 (br), 33.56 (br), 25.90 (br), 12.18 (br), 9.55 (br), 3.02 (br), 1.14 (br), −0.89 (br), −2.58 (br), −4.68 (br), −13.10 (br), −29.99 (br), −70.66 (br), −81.45 (br), −88.74 (br). Anal. Calcd for $C_{45}H_{58}FeN_4$: C 76.04, H 8.22, N 7.88; Found: C 75.86, H 7.84, N 7.75. Magnetic susceptibility (C_6D_6, 302 K): μ_{eff} = 4.8(2) μ_B. Absorption spectrum (THF): λ_{max}, nm (ε, M^{-1} cm^{-1}) = 290 (6100). IR (KBr, cm^{-1}): ν = 3344 (w), 2960 (s), 2921 (m), 2867 (m), 1693 (s), 1613 (m), 1541 (w), 1489 (m), 1459 (s), 1439 (s), 1382 (w), 1361 (w), 1263 (m), 1233 (m), 1164 (w), 1111 (w), 1045 (m), 927 (w), 908 (w), 852 (m), 791 (w), 744 (s), 570 (w).

Quenching Reaction of 7. An Et_2O (5 mL) solution of **7** (102 mg, 0.14 mmol) was quenched with H_2O (1 mL). Then, the mixture was extracted with CH_2Cl_2 (15 mL × 3) and the combined organic phases were dried over Na_2SO_4. After filtration and removal of volatiles, flash column chromatography (silica gel, CH_2Cl_2) afforded a yellow oil. GC-MS and ^{1}H NMR analyses with the addition of 1,3,5-trimethoxybenzene (11 mg, 0.064 mmol) as an internal standard indicated the formation of $H_2NC_6H_3$-2-Pr^i-6-CMe=CH_2 (0.09 mmol) and $DippNH_2$ (0.13 mmol). For $H_2NC_6H_3$-2-Pr^i-6-CMe=CH_2: ^{1}H NMR (400 MHz, $CDCl_3$, 294 K): δ (ppm) 5.34−5.31 (m, 1H, =CH_2), 5.08−5.05 (m, 1H, C=CH_2), 2.11−2.08 (m, 3H, =CCH_3).

Reaction of 1 with $PhSiH_3$. To a red solution of **1** (209 mg, 0.29 mmol) in toluene (5 mL) was added $PhSiH_3$ (71 mg, 0.66 mmol) at room temperature. The reaction mixture was stirred for 24 h, and the color of the solution changed from red to orange gradually. Removal of the solvent under a vacuum afforded an orange solid. The residue was washed with *n*-hexane (5 mL) and then extracted with Et_2O (5 mL). The extract was filtered to afford an orange solution. Slow evaporation of the solvent at room temperature afforded [(IMes)Fe-(NHDipp)(NDippSiPhH_2)] (**8**) as orange crystals suitable for X-ray crystallography (112 mg, 47%). ^{1}H NMR (300 MHz, C_6D_6, 302 K): δ (ppm) 64.85 (br), 45.29 (br), 11.14 (br), 3.51 (br), −3.04 (br), −3.38 (br), −5.48 (br), −13.02 (br), −26.44 (br), −85.22 (br). Anal. Calcd for $C_{51}H_{66}FeN_4Si$: C, 74.79; H, 8.12; N, 6.84. Found: C, 74.70; H, 8.08; N, 7.00. Magnetic susceptibility (C_6D_6, 295 K): μ_{eff} = 5.4(1) μ_B. Absorption spectrum (THF): λ_{max}, nm (ε, M^{-1} cm^{-1}) = 289 (6900), 342 (1300). IR (KBr, cm^{-1}): ν = 3370 (w), 3043 (w), 2960 (s), 2868 (m), 2110 (m), 1691 (s), 1621 (m), 1588 (w), 1544 (w), 1486 (m), 1460 (s), 1439 (s), 1382 (w), 1359 (w), 1335 (w), 1263 (m), 1231 (m), 1184 (w), 1114 (m), 1040 (m), 915 (s), 888 (m), 851 (s), 778 (w), 741 (m), 711 (m), 570 (w).

Reaction of 1 with PhN=C=NPh. To a red solution of **1** (133 mg, 0.19 mmol) in toluene (5 mL) was added PhN=C=NPh (45 mg, 0.23 mmol) at room temperature. The reaction mixture was stirred for 5 min, and the color of the solution changed from red to dark red immediately. Removal of the solvent under a vacuum afforded a dark red solid. The residue was washed with *n*-hexane (5 mL) and then extracted with a mixture of Et_2O/*n*-hexane (2:1, 5 mL) and filtered. Recrystallization of the crude product from the Et_2O/*n*-hexane solution at −35 °C afforded [(IMes)Fe(NDipp)(N(Dipp)C(NPh)(=NPh))] (**9**) as dark red crystals suitable for X-ray crystallography (98 mg, 58%). ^{1}H NMR (400 MHz, C_6D_6, 292 K): δ (ppm) 57.25 (br), 50.48 (br), 39.21 (br), 28.16 (br), 21.66 (br), 20.72 (br), 11.85 (br), 10.00 (br), 7.75 (br), 5.62 (br), 2.14 (br), 1.48 (br), −0.85 (br), −5.02 (br), −10.02 (br), −12.93 (br), −15.99 (br), −45.63 (br), −76.99 (br), −92.08 (br). Anal. Calcd for $C_{58}H_{68}FeN_6$: C, 76.97; H, 7.57; N, 9.29. Found: C, 76.59; H, 7.23; N, 9.10. Magnetic susceptibility (C_6D_6, 295 K): μ_{eff} = 4.1(1) μ_B. Absorption spectrum (THF): λ_{max}, nm (ε, M^{-1} cm^{-1}) = 477 (2200), 714 (980). IR (KBr, cm^{-1}): ν = 2968 (s), 2873 (m), 1654 (s), 1598 (s), 1586 (s), 1536 (s), 1495 (s), 1442 (s), 1381 (m), 1315 (m), 1255 (m), 1233 (m), 1109 (w), 1034 (w), 926 (w), 853 (m), 754 (m), 696 (m), 572 (w).

Reaction of 1 with *p*-Pr^iC_6H_4NCO. To a red solution of **1** (352 mg, 0.50 mmol) in toluene (10 mL) was added *p*-Pr^iC_6H_4NCO (81 mg, 0.50 mmol) at room temperature. The reaction mixture was stirred for 5 min, and the color of the solution changed from red to dark brown immediately. Removal of the solvent under a vacuum afforded a brown solid. The solid was washed with *n*-hexane (10 mL) and dried under a vacuum to give a crude product of [(IMes)Fe-(NDipp)(N(Dipp)C(O)N(*p*-Pr^iC_6H_4))] (**10**) as a brown solid (372 mg, 86%). The product was further purified via recrystallization in an Et_2O/*n*-hexane (2:1) solution at −35 °C. ^{1}H NMR (400 MHz, C_6D_6, 292 K): δ (ppm) 44.36 (br), 40.84 (br), 37.79 (br), 37.10 (br), 18.43 (br), 9.44 (br), 8.56 (br), 5.46 (br), 4.25 (br), 4.11 (br), 4.00 (br), 3.51 (br), 2.71 (br), 2.53 (br), 1.87 (br), 0.67 (br), −0.35 (br), −5.55 (br), −21.76 (br), −57.65 (br), −67.54 (br). Anal. Calcd for $C_{55}H_{69}FeN_5O$: C, 75.75; H, 7.98; N, 8.03. Found: C, 75.32; H, 8.16; N, 7.61. Magnetic susceptibility (C_6D_6, 295 K): μ_{eff} = 4.0(1) μ_B. Absorption spectrum (THF): λ_{max}, nm (ε, M^{-1} cm^{-1}) = 281 (9400), 620 (1100). IR (KBr, cm^{-1}): ν = 2958 (s), 2923 (s), 2865 (s), 1702 (w), 1628 (m), 1505 (m), 1486 (m), 1459 (m), 1379 (w), 1310 (m), 1255 (m), 1101 (w), 1054 (w), 1035 (w), 928 (w), 850 (m), 832 (m), 798 (w), 760 (m), 744 (m), 551 (m).

Quenching Reaction of 10. An Et_2O solution of **10** (134 mg, 0.15 mmol) was quenched with H_2O. The mixture was then extracted

DOI: 10.1021/jacs.5b09579
J. Am. Chem. Soc. 2015, 137, 14196−14207

with CH_2Cl_2 (15 mL × 3), and the combined organic phases were dried over Na_2SO_4. After filtration and removal of volatiles, flash column chromatography (silica gel, 1:1 *n*-hexane/CH_2Cl_2) afforded DippHNC(O)NH(C_6H_4-*p*-Pr^i) as a white solid (40 mg, 77%). ^{1}H NMR (400 MHz, DMSO-d_6, 292 K): δ (ppm) 8.64 (br, 1H, N*H*), 7.61 (br, 1H, N*H*), 7.37 (d, J = 8.5 Hz, 2H, *m*-C_6H_3), 7.29−7.24 (m, 1H, *p*-C_6H_3), 7.19−7.11 (m, 4H, C_6H_4), 3.19 (hept, J = 6.8 Hz, 2H, $CH(CH_3)_2$), 2.83 (hept, J = 6.7 Hz, 1H, $CH(CH_3)_2$), 1.21−1.15 (m, 18H, CH_3). ^{13}C NMR (101 MHz, DMSO-d_6, 292 K): δ (ppm) 154.79, 147.07, 141.76, 138.52, 132.91, 127.60, 126.83, 123.30, 118.31, 33.21, 28.44, 24.52, 24.34, 23.69. IR (thin film): ν = 3301 (w), 2958 (w), 2927 (w), 2867 (w), 1642 (m), 1596 (m), 1553 (s), 1514 (m), 1467 (w), 1413 (w), 1307 (m), 1233 (m), 1056 (w), 831 (w), 787 (m), 725 (m), 668 (m). HRMS (ESI): calcd for $C_{22}H_{31}N_2O$ [(M+H)$^+$], 339.2436; found, 339.2428.

Reaction of 1 with CO. A red solution of **1** (70 mg, 0.098 mmol) in Et_2O (10 mL) was cooled with liquid N_2, and then CO was introduced to the mixture via a CO balloon (1 atm). The mixture was allowed to warm to room temperature and stirred for 12 h, giving a brown-yellow solution. Removal of the solvent under a vacuum afforded a brown residue that was washed with *n*-hexane (10 mL) and filtered. The solid residue was collected and dried under a vacuum to afford [(IMes)Fe(CO)$_4$] as a yellow solid (30 mg, 64%). The *n*-hexane solution was analyzed by GC-MS and ^{1}H NMR spectroscopy with 1,3,5-trimethoxybenzene as the internal standard (26 mg, 0.15 mmol), which indicated the formation of DippNCO in 71% yield. For [(IMes)Fe(CO)$_4$]:[24] ^{1}H NMR (400 MHz, C_6D_6, 292 K): δ (ppm) 6.78 (s, 4H, *m*-C_6H_2), 6.14 (s, 2H, =C*H*), 2.11 (s, 6H, CH_3), 2.04 (s, 12H, CH_3). ^{13}C NMR (101 MHz, C_6D_6, 292 K): δ (ppm) 216.82 (CO), 187.31 ($C_{carbene}$), 139.17, 136.90, 135.67, 129.36, 124.05, 20.77, 17.83. IR (KBr, cm^{-1}): ν = 2963 (w), 2040 (m), 1951 (m), 1920 (s), 1611 (w), 1488 (w), 1399 (w), 1306 (w), 1264 (w), 1084 (w), 705 (w), 626 (w). For DippNCO: ^{1}H NMR (400 MHz, C_6D_6, 295 K): δ (ppm) 6.89−7.01 (m, 3H, Dipp-C*H*), 3.14−3.03 (m, 2H, $CH(CH_3)_2$), 1.07 (d, J = 6.8 Hz, 6H, $CH(CH_3)_2$). The ^{1}H NMR spectrum is identical to that reported in the literature.[55]

Reaction of 1 with Bu^{t}NC. A J-Young NMR tube was charged with 1,3,5-trimethoxybenzene (12 mg, 0.072 mmol), **1** (16 mg, 0.023 mmol), and C_6D_6 (0.5 mL) at room temperature, and then Bu^{t}NC (17 mg, 0.20 mmol) was added. The color of the mixture changed from red to orange quickly. After 1 h, the ^{1}H NMR signals of **1** disappeared, and new signals arising from DippNCNBu^t appeared. ^{1}H NMR spectroscopy with 1,3,5-trimethoxybenzene as the internal standard indicated the formation of the carbodiimide in 70% yield. For DippNCNBu^t: ^{1}H NMR (400 MHz, C_6D_6, 293 K): δ (ppm) 7.05 (s, 3H, Dipp-C*H*), 3.68−3.56 (m, 2H, $CH(CH_3)_2$), 1.28 (s, 9H, CH_3), 1.23 (d, J = 6.8 Hz, 6H, $CH(CH_3)_2$). The ^{1}H NMR spectrum is identical to that reported in the literature.[56]

Computational Details. All molecular geometries were optimized in the gas phase, employing TPSS[57] density functional with def2-SVP basis set[58] for all atoms. Optimized minima and transition states were verified by harmonic vibrational analysis to have no and one proper imaginary frequency, respectively. To refine the calculated energy, single-point calculations with larger basis sets were then done, based on these optimized structures, by using TPSS functional with def2-TZVP basis set.[58] The solvent effect was modeled in these single-point calculations by employing the continuum solvation model of SMD[59] with toluene as the solvent. The free energies reported in this work were calculated at the TPSS/def2-TZVP level, including the Gibbs free energy thermal correction obtained from vibrational analysis in the gas phase, as well as Grimme's DFT empirical dispersion correction, DFT-D3, with Grimme's original short-range damping.[60] ^{57}Fe Mössbauer spectroscopic parameters were calculated by employing TPSS functional with CP(PPP)[61] basis set for Fe, def2-TZVP basis set for the first coordination sphere, and def2-SV(P) basis set for the rest of the atoms. All geometry optimizations and single-point calculations were performed with the Gaussian 09 program.[62] ^{57}Fe Mössbauer spectroscopic parameter calculations were done with ORCA program package.[63]

■ ASSOCIATED CONTENT

Supporting Information

The Supporting Information is available free of charge on the ACS Publications website at DOI: 10.1021/jacs.5b09579.

^{57}Fe Mössbauer spectra, absorption spectra, NMR spectra, spin populations of the calculated structures, and calculated reaction profiles of other unfavorable reaction pathways (PDF)

X-ray crystallographic data for **4**−**9** (CIF)

Cartesian coordinates of the optimized structure in the route of the dehydrogenation reaction (XYZ)

Cartesian coordinates of the optimized structure in the route of the reaction of **1** with $PhSiH_3$ (XYZ)

■ AUTHOR INFORMATION

Corresponding Authors

*chenh@iccas.ac.cn

*deng@sioc.ac.cn

Author Contributions

§L.W. and L.H. contributed equally.

Notes

The authors declare no competing financial interest.

■ ACKNOWLEDGMENTS

The work was supported by the National Natural Science Foundation of China (Nos. 21222208, 21421091, and 21432001 to L.D., and Nos. 21290194, 21221002, and 21473215 to H.C.).

■ REFERENCES

(1) Peters, J. W.; Szilagyi, R. K. *Curr. Opin. Chem. Biol.* **2006**, *10*, 101.

(2) (a) Che, C.-M.; Zhou, C.-Y.; Wong, E. L.-M. *Top. Organomet. Chem.* **2011**, *33*, 111. (b) Zhang, L.; Deng, L. *Chin. Sci. Bull.* **2012**, *57*, 2352.

(3) Liu, G.-S.; Zhang, Y.-Q.; Yuan, Y.-A.; Xu, H. *J. Am. Chem. Soc.* **2013**, *135*, 3343.

(4) Eikey, R. A.; Abu-Omar, M. M. *Coord. Chem. Rev.* **2003**, *243*, 83.

(5) Verma, A. K.; Nazif, T. N.; Achim, C.; Lee, S. C. *J. Am. Chem. Soc.* **2000**, *122*, 11013.

(6) For reviews on iron imido complexes, see ref 2 and the following: (a) Mehn, M. P.; Peters, J. C. *J. Inorg. Biochem.* **2006**, *100*, 634. (b) Berry, J. F. *Comments Inorg. Chem.* **2009**, *30*, 28. (c) Saouma, C. T.; Peters, J. C. *Coord. Chem. Rev.* **2011**, *255*, 920.

(7) (a) Svastits, E. W.; Dawson, J. H.; Breslow, R.; Gellman, S. H. *J. Am. Chem. Soc.* **1985**, *107*, 6427. (b) Farwell, C. C.; Zhang, R. K.; McIntosh, J. A.; Hyster, T. K.; Arnold, F. H. *ACS Cent. Sci.* **2015**, *1*, 89.

(8) (a) Brown, S. D.; Betley, T. A.; Peters, J. C. *J. Am. Chem. Soc.* **2003**, *125*, 322. (b) Betley, T. A.; Peters, J. C. *J. Am. Chem. Soc.* **2003**, *125*, 10782. (c) Brown, S. D.; Peters, J. C. *J. Am. Chem. Soc.* **2004**, *126*, 4538.

(9) (a) Eckert, N. A.; Vaddadi, S.; Stoian, S.; Lachicotte, R. J.; Cundari, T. R.; Holland, P. L. *Angew. Chem., Int. Ed.* **2006**, *45*, 6868. (b) Cowley, R. E.; Eckert, N. A.; Elhaïk, J.; Holland, P. L. *Chem. Commun.* **2009**, 1760. (c) Cowley, R. E.; DeYonker, N. J.; Eckert, N. A.; Cundari, T. R.; Debeer, S.; Bill, E.; Ottenwaelder, X.; Flaschenriem, C.; Holland, P. L. *Inorg. Chem.* **2010**, *49*, 6172. (d) Cowley, R. E.; Eckert, N. A.; Vaddadi, S.; Figg, T. M.; Cundari, T. R.; Holland, P. L. *J. Am. Chem. Soc.* **2011**, *133*, 9796.

(10) (a) Kuppuswamy, S.; Powers, T. M.; Johnson, B. M.; Bezpalko, M. W.; Brozek, C. K.; Foxman, B. M.; Berben, L. A.; Thomas, C. M. *Inorg. Chem.* **2013**, *52*, 4802. (b) Kuppuswamy, S.; Powers, T. M.; Johnson, B. M.; Brozek, C. K.; Krogman, J. P.; Bezpalko, M. W.; Berben, L. A.; Keith, J. M.; Foxman, B. M.; Thomas, C. M. *Inorg. Chem.* **2014**, *53*, 5429.

DOI: 10.1021/jacs.5b09579
J. Am. Chem. Soc. 2015, 137, 14196−14207

(11) (a) Bart, S. C.; Lobkovsky, E.; Bill, E.; Chirik, P. J. *J. Am. Chem. Soc.* **2006**, *128*, 5302. (b) Bowman, A. C.; Milsmann, C.; Bill, E.; Turner, Z. R.; Lobkovsky, E.; Debeer, S.; Wieghardt, K.; Chirik, P. J. *J. Am. Chem. Soc.* **2011**, *133*, 17353.
(12) (a) Brown, S. D.; Peters, J. C. *J. Am. Chem. Soc.* **2005**, *127*, 1913. (b) Moret, M.-E.; Peters, J. C. *Angew. Chem., Int. Ed.* **2011**, *50*, 2063.
(13) Thomas, C. M.; Mankad, N. P.; Peters, J. C. *J. Am. Chem. Soc.* **2006**, *128*, 4956.
(14) Nieto, I.; Ding, F.; Bontchev, R. P.; Wang, H.; Smith, J. M. *J. Am. Chem. Soc.* **2008**, *130*, 2716.
(15) Klinker, E. J.; Jackson, T. A.; Jensen, M. P.; Stubna, A.; Juhász, G.; Bominaar, E. L.; Münck, E.; Que, L., Jr. *Angew. Chem., Int. Ed.* **2006**, *45*, 7394.
(16) (a) King, E. R.; Hennessy, E. T.; Betley, T. A. *J. Am. Chem. Soc.* **2011**, *133*, 4917. (b) Hennessy, E. T.; Betley, T. A. *Science* **2013**, *340*, 591. (c) Hennessy, E. T.; Liu, R. Y.; Iovan, D. A.; Duncan, R. A.; Betley, T. A. *Chem. Sci.* **2014**, *5*, 1526.
(17) Searles, K.; Fortier, S.; Khusniyarov, M. M.; Carroll, P. J.; Sutter, J.; Meyer, K.; Mindiola, D. J.; Caulton, K. G. *Angew. Chem., Int. Ed.* **2014**, *53*, 14139.
(18) Ni, C.; Fettinger, J. C.; Long, G. J.; Brynda, M.; Power, P. P. *Chem. Commun.* **2008**, 6045.
(19) Zhang, H.; Ouyang, Z.; Liu, Y.; Zhang, Q.; Wang, L.; Deng, L. *Angew. Chem., Int. Ed.* **2014**, *53*, 8432.
(20) For examples of low-spin iron−NHC complexes, see: (a) Fränkel, R.; Kernbach, U.; Bakola-Christianopoulou, M.; Plaia, U.; Suter, M.; Ponikwar, W.; Nöth, H.; Moinet, C.; Fehlhammer, W. P. *J. Organomet. Chem.* **2001**, *617*−*618*, 530. (b) Mercs, L.; Labat, G.; Neels, A.; Ehlers, A.; Albrecht, M. *Organometallics* **2006**, *25*, 5648. (c) Liu, T.; Darensbourg, M. Y. *J. Am. Chem. Soc.* **2007**, *129*, 7008. (d) Liu, B.; Xia, Q.; Chen, W. *Angew. Chem., Int. Ed.* **2009**, *48*, 5513. (e) Blom, B.; Tan, G.; Enthaler, S.; Inoue, S.; Epping, J. D.; Driess, M. *J. Am. Chem. Soc.* **2013**, *135*, 18108. (f) Meyer, S.; Klawitter, I.; Demeshko, S.; Bill, E.; Meyer, F. *Angew. Chem., Int. Ed.* **2013**, *52*, 901. (g) Hashimoto, T.; Hoshino, R.; Hatanaka, T.; Ohki, Y.; Tatsumi, K. *Organometallics* **2014**, *33*, 921.
(21) Hendrich, M. P.; Gunderson, W.; Behan, R. K.; Green, M. T.; Mehn, M. P.; Betley, T. A.; Lu, C. C.; Peters, J. C. *Proc. Natl. Acad. Sci. U. S. A.* **2006**, *103*, 17107.
(22) Vogel, C.; Heinemann, F. W.; Sutter, J.; Anthon, C.; Meyer, K. *Angew. Chem., Int. Ed.* **2008**, *47*, 2681.
(23) (a) Mo, Z.; Ouyang, Z.; Wang, L.; Fillman, K. L.; Neidig, M. L.; Deng, L. *Org. Chem. Front.* **2014**, *1*, 1040. (b) Lavallo, V.; Canac, Y.; Präsang, C.; Donnadieu, B.; Bertrand, G. *Angew. Chem., Int. Ed.* **2005**, *44*, 5705. (c) Back, O.; Henry-Ellinger, M.; Martin, C. D.; Martin, D.; Bertrand, G. *Angew. Chem., Int. Ed.* **2013**, *52*, 2939.
(24) Zhang, L.; Liu, Y.; Deng, L. *J. Am. Chem. Soc.* **2014**, *136*, 15525.
(25) (a) Krebs, C.; Fujimori, D. G.; Walsh, C. T.; Bollinger, J. M., Jr. *Acc. Chem. Res.* **2007**, *40*, 484. (b) Shanklin, J.; Guy, J. E.; Mishra, G.; Lindqvist, Y. *J. Biol. Chem.* **2009**, *284*, 18559.
(26) Mukherjee, A.; Martinho, M.; Bominaar, E. L.; Münck, E.; Que, L., Jr. *Angew. Chem., Int. Ed.* **2009**, *48*, 1780.
(27) Lucas, R. L.; Powell, D. R.; Borovik, A. S. *J. Am. Chem. Soc.* **2005**, *127*, 11596.
(28) For an early review on transition metal imido complexes, see: Wigley, D. E. *Prog. Inorg. Chem.* **1994**, *42*, 239.
(29) For examples, see: (a) Gountchev, T. I.; Tilley, T. D. *J. Am. Chem. Soc.* **1997**, *119*, 12831. (b) Ignatov, S. K.; Rees, N. H.; Dubberley, S. R.; Razuvaev, A. G.; Mountford, P.; Nikonov, G. I. *Chem. Commun.* **2004**, 952.
(30) Suess, D. L. M.; Peters, J. C. *J. Am. Chem. Soc.* **2013**, *135*, 4938.
(31) Du, J.; Wang, L.; Xie, M.; Deng, L. *Angew. Chem., Int. Ed.* **2015**, *54*, 12640.
(32) For examples, see: (a) Zuckerman, R. L.; Bergman, R. G. *Organometallics* **2000**, *19*, 4795. (b) Ong, T.-G.; Yap, G. P. A.; Richeson, D. S. *J. Am. Chem. Soc.* **2003**, *125*, 8100. (c) Chu, J.; Lu, E.; Liu, Z.; Chen, Y.; Leng, X.; Song, H. *Angew. Chem., Int. Ed.* **2011**, *50*, 7677.
(33) Glueck, D. S.; Hollander, F. J.; Bergman, R. G. *J. Am. Chem. Soc.* **1989**, *111*, 2719.
(34) Mindiola, D. J.; Waterman, R.; Iluc, V. M.; Cundari, T. R.; Hillhouse, G. L. *Inorg. Chem.* **2014**, *53*, 13227.
(35) The complex can be viewed as an iron(IV) species (S = 1 or 2) or an iron(III) species (S = 3/2 or 5/2) having an antiferromagnetically coupled imido radical ligand, $[NDipp]^{\bullet-}$. Its detailed electronic structure necessitates further detailed spectroscopic study.
(36) Warratz, S.; Postigo, L.; Royo, B. *Organometallics* **2013**, *32*, 893.
(37) Iron(0) isocyanide complexes might undergo C−NC bond cleavage reactions. For example, see: Halbauer, K.; Dönnecke, D.; Görls, H.; Imhof, W. *Z. Anorg. Allg. Chem.* **2006**, *632*, 1477.
(38) (a) Chong, A. O.; Oshima, K.; Sharpless, K. B. *J. Am. Chem. Soc.* **1977**, *99*, 3420. (b) Muñiz, K. *New J. Chem.* **2005**, *29*, 1371. (c) Cardona, F.; Goti, A. *Nat. Chem.* **2009**, *1*, 269.
(39) See the Experimental Section for computational details.
(40) For some reviews of computational studies on C−H activation by first-row late transition metal oxo, imido, and carbene complexes, see: (a) Decker, A.; Solomon, E. I. *Curr. Opin. Chem. Biol.* **2005**, *9*, 152. (b) Shaik, S.; Kumar, D.; de Visser, S. P.; Altun, A.; Thiel, W. *Chem. Rev.* **2005**, *105*, 2279. (c) Bassan, A.; Blomberg, M. R. A.; Borowski, T.; Siegbahn, P. E. M. *J. Inorg. Biochem.* **2006**, *100*, 727. (d) Ye, S.; Neese, F. *Curr. Opin. Chem. Biol.* **2009**, *13*, 89. (e) Balcells, D.; Clot, E.; Eisenstein, O. *Chem. Rev.* **2010**, *110*, 749. (f) Shaik, S.; Chen, H.; Janardanan, D. *Nat. Chem.* **2011**, *3*, 19. (g) Li, D.; Wang, Y.; Han, K. *Coord. Chem. Rev.* **2012**, *256*, 1137. (h) Lundberg, M.; Borowski, T. *Coord. Chem. Rev.* **2013**, *257*, 277. (i) Saouma, C. T.; Mayer, J. M. *Chem. Sci.* **2014**, *5*, 21.
(41) For selected examples of computational studies on C−H activation by first-row late transition metal imido complexes, see refs 9a,d and the following: (a) Badiei, Y. M.; Dinescu, A.; Dai, X.; Palomino, R. M.; Heinemann, F. W.; Cundari, T. R.; Warren, T. H. *Angew. Chem., Int. Ed.* **2008**, *47*, 9961. (b) Cundari, T. R.; Jimenez-Halla, J. O. C.; Morello, G. R.; Vaddadi, S. *J. Am. Chem. Soc.* **2008**, *130*, 13051. (c) Olatunji-Ojo, O. A.; Cundari, T. R. *Inorg. Chem.* **2013**, *52*, 8106. (d) Pierpont, A. W.; Cundari, T. R. *Inorg. Chem.* **2010**, *49*, 2038. (e) Wiese, S.; McAfee, J. L.; Pahls, D. R.; McMullin, C. L.; Cundari, T. R.; Warren, T. H. *J. Am. Chem. Soc.* **2012**, *134*, 10114. (f) Cundari, T. R.; Klinckman, T. R.; Wolczanski, P. T. *J. Am. Chem. Soc.* **2002**, *124*, 1481. (g) Iluc, V. M.; Hillhouse, G. L. *J. Am. Chem. Soc.* **2010**, *132*, 15148. (h) Kumar, S.; Faponle, A. S.; Barman, P.; Vardhaman, A. K.; Sastri, C. V.; Kumar, D.; de Visser, S. P. *J. Am. Chem. Soc.* **2014**, *136*, 17102.
(42) Several other comparatively unfavorable pathways of dehydrogenation reaction from **1** have also been considered in our calculations, including (1) HAA from a benzylic position of Dipp by the imido N atom of the other Dipp group; (2) HAA from a methyl group of Dipp by either N atom of the two imido groups; (3) 1,2-addition of the two adjacent benzylic and methyl H atoms in one Dipp to its imido N atom and Fe atom, respectively, followed by H-migration from Fe to the imido N atom of the other Dipp group; (4) 1,2-addition of the two adjacent benzylic and methyl H atoms in one Dipp to the imido N atom of the other Dipp group and Fe atom, respectively; (5) HAA from a benzylic position of Dipp by the Fe atom; (6) synergistic activation of two adjacent benzylic and methyl C−H bonds in Dipp by two imido N atoms to directly generate product **7**; and (7) direct generation of product **7** via HAA from the methyl position adjacent to the benzylic radical by the imido N atom of the other Dipp group after **11** is generated through $\mathbf{TS}_{1-11}$ as shown in Figure 8. All these pathways were found to have higher energies than the pathway shown in Figure 7. See Figures S29−S35 for more details.
(43) (a) Mayer, J. M. *Acc. Chem. Res.* **1998**, *31*, 441. (b) Lai, W.; Li, C.; Chen, H.; Shaik, S. *Angew. Chem., Int. Ed.* **2012**, *51*, 5556.
(44) (a) Schröder, D.; Shaik, S.; Schwarz, H. *Acc. Chem. Res.* **2000**, *33*, 139. (b) Shaik, S.; Hirao, H.; Kumar, D. *Acc. Chem. Res.* **2007**, *40*, 532.
(45) Several other comparatively unfavorable pathways of reaction of **1** with $PhSiH_3$ have also been considered in our calculations, including (1) HAA from $PhSiH_3$ by an imido N atom to generate silyl radical;

DOI: 10.1021/jacs.5b09579
J. Am. Chem. Soc. 2015, 137, 14196−14207

(2) HAA from a $PhSiH_3$ by Fe atom to generate silyl radical; and (3) synergistic activation of Si−H bond by two imido N atoms to directly generate product **8**. These pathways were found either to have higher energy than the pathway shown in Figure 9 (pathways (1) and (2)) or to fail to link the reactant and product (pathway (3)). See Figures S36 and S37 for more details.
(46) (a) Shaik, S.; Cohen, S.; Wang, Y.; Chen, H.; Kumar, D.; Thiel, W. *Chem. Rev.* **2010**, *110*, 949. (b) Nam, W. *Acc. Chem. Res.* **2007**, *40*, 522. (c) Costas, M.; Mehn, M. P.; Jensen, M. P.; Que, L., Jr. *Chem. Rev.* **2004**, *104*, 939.
(47) Jafarpour, L.; Stevens, E. D.; Nolan, S. P. *J. Organomet. Chem.* **2000**, *606*, 49.
(48) Nguyen, Q.; Sun, K.; Driver, T. G. *J. Am. Chem. Soc.* **2012**, *134*, 7262.
(49) Radziszewski, J. G.; Downing, J. W.; Jawdosiuk, M.; Kovacic, P.; Michl, J. *J. Am. Chem. Soc.* **1985**, *107*, 594.
(50) Hassner, A.; Fibiger, R.; Andisik, D. *J. Org. Chem.* **1984**, *49*, 4237.
(51) Ali, A. R.; Ghosh, H.; Patel, B. K. *Tetrahedron Lett.* **2010**, *51*, 1019.
(52) (a) Evans, D. F. *J. Chem. Soc.* **1959**, 2003. (b) Sur, S. K. *J. Magn. Reson.* **1989**, *82*, 169.
(53) Sheldrick, G. M. *SADABS*: Program for Empirical Absorption Correction of Area Detector Data; University of Göttingen: Göttingen, Germany, 1996.
(54) Sheldrick, G. M. *SHELXTL 5.10 for Windows NT*: Structure Determination Software Programs; Bruker Analytical X-ray Systems, Inc.: Madison, WI, USA, 1997.
(55) For data of DippNCO, see: Kilgore, U. J.; Basuli, F.; Huffman, J. C.; Mindiola, D. J. *Inorg. Chem.* **2006**, *45*, 487.
(56) For data of DippNCNBu^t, see: Blom, B.; Pohl, M.; Tan, G.; Gallego, D.; Driess, M. *Organometallics* **2014**, *33*, 5272.
(57) Tao, J.; Perdew, J. P.; Staroverov, V. N.; Scuseria, G. E. *Phys. Rev. Lett.* **2003**, *91*, 146401.
(58) Weigend, F.; Ahlrichs, R. *Phys. Chem. Chem. Phys.* **2005**, *7*, 3297.
(59) Marenich, A. V.; Cramer, C. J.; Truhlar, D. G. *J. Phys. Chem. B* **2009**, *113*, 6378.
(60) (a) Grimme, S.; Antony, J.; Ehrlich, S.; Krieg, H. *J. Chem. Phys.* **2010**, *132*, 154104. (b) Goerigk, L.; Grimme, S. *J. Chem. Theory Comput.* **2011**, *7*, 291.
(61) Neese, F. *Inorg. Chim. Acta* **2002**, *337*, 181.
(62) Frisch, M. J.; Trucks, G. W.; Schlegel, H. B.; Scuseria, G. E.; Robb, M. A.; Cheeseman, J. R.; Scalmani, G.; Barone, V.; Mennucci, B.; Petersson, G. A.; Nakatsuji, H.; Caricato, M.; Li, X.; Hratchian, H. P.; Izmaylov, A. F.; Bloino, J.; Zheng, G.; Sonnenberg, J. L.; Hada, M.; Ehara, M.; Toyota, K.; Fukuda, R.; Hasegawa, J.; Ishida, M.; Nakajima, T.; Honda, Y.; Kitao, O.; Nakai, H.; Vreven, T.; Montgomery, J. A., Jr.; Peralta, J. E.; Ogliaro, F.; Bearpark, M.; Heyd, J. J.; Brothers, E.; Kudin, K. N.; Staroverov, V. N.; Kobayashi, R.; Normand, J.; Raghavachari, K.; Rendell, A.; Burant, J. C.; Iyengar, S. S.; Tomasi, J.; Cossi, M.; Rega, N.; Millam, J. M.; Klene, M.; Knox, J. E.; Cross, J. B.; Bakken, V.; Adamo, C.; Jaramillo, J.; Gomperts, R.; Stratmann, R. E.; Yazyev, O.; Austin, A. J.; Cammi, R.; Pomelli, C.; Ochterski, J. W.; Martin, R. L.; Morokuma, K.; Zakrzewski, V. G.; Voth, G. A.; Salvador, P.; Dannenberg, J. J.; Dapprich, S.; Daniels, A. D.; Farkas, O.; Foresman, J. B.; Ortiz, J. V.; Cioslowski, J.; Fox, D. J. *Gaussian 09*, revision C.01; Gaussian, Inc.: Wallingford, CT, 2009.
(63) Neese, F. *ORCA*: an ab initio, density functional and semiempirical program package, version 2.6.35; University of Bonn: Bonn, Germany, March 2008; http://www.thch.uni-bonn.de/tc/orca/.

DOI: 10.1021/jacs.5b09579
J. Am. Chem. Soc. 2015, 137, 14196−14207